e-ISSN: 2146 - 9067

International Journal of Automotive Engineering and Technologies

journal homepage:
https://dergipark.org.tr/en/pub/ijaet

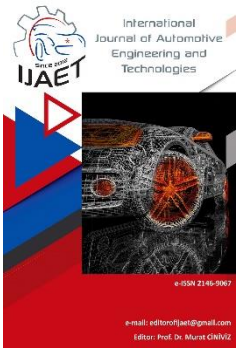

Original Research Article

Suspension system design for pedal-assisted cargo E-quadricycle

Mehmet Onur Genç [1, *]

[1, *]Department of Mechatronics Engineering, Bursa Technical University, Türkiye.

ARTICLE INFO

Orcid Numbers
1. 0000-0003-0332-1785

Doi: 10.18245/ijaet.1290044

* Corresponding author
onur.genc@btu.edu.tr

Received: Apr 30, 2023
Accepted: Jan 29, 2024

Published: 27 Mar 2024

Published by Editorial Board Members of IJAET

ABSTRACT

Electro Micro-Mobility (EMM) has widely increased in Today's transportation preferences. The suspension system design based on the road profile in E-Quadricycle needs further investigation to present more optimized EMM vehicles soon. In this study, the pedal-assisted Cargo E-Quadricycle is investigated based on powertrain system modeling considering suspension system design. System modeling is applied to have an optimized suspension system design specified for Cargo E-Quadricycle to provide more comfortable driving. To achieve these targets, one-dimensional physical modeling is obtained, and the key parameters for system design are defined based on the State-space system modeling definition. In the next phase, the suspension system is constructed as a passive-controlled type with assigned suspension parameters considering natural frequency to provide driving comfort in urban transportation. Because four-wheeler Pedal-Assisted Cargo E-Quadricycles have specific vehicle kinematics and dynamics based on their own limited acceleration system and vehicle design, this study presents the suspension system design steps and remarkable dynamic concerns.

Keywords: E-Quadricycle, E-Mobility, Suspension, System Modeling..

1. Introduction

E-Mobility widely increases its preferences among people day by day. EMM vehicles are more in demand in terms of lithium-ion battery usage compared to classical E-Mobility vehicles due to less amount of product life cycles based on cell quantities. Electrification in transportation increased its spread after the 2020s due to economic and commercial changes in the World. Climatic concerns are also important points in changing general tendencies for people and societies to change their habits. Because of these factors, preferences for using combustion engines in urban transportation and commercial areas have recently started to change. Micro Electro Mobility (EMM) emerged also for the alternative E-Mobility, especially in urban transportation over short distances. One of the advantages of EMM vehicles are economical both in vehicle cost and energy source cost. Lithium-ion pedal-assisted E-Mobility Quadricycle vehicles need consideration based

on the pedal assist system calculation to model the powertrain system. In this study, the pedal-assisted cargo E-Quadricycle is investigated based on system modeling and suspension system design by considering constructive and environmental boundary conditions. Figure 1 shows the pedal-assisted cargo E-Quadricycles designed for this study. E-quadricycles correspond to a vehicle having a four-wheel excited with an electric motor. Pedal-assisted E-Quadricycles are also controlled and driven by pedal force. The designed cargo model in this study considers the urban cargo activities with an additional 80 kg carrying effective limit. This kind of model can be presented to the market consumption sector, cargo delivery, and also the company's internal transportation activities. These vehicles also comply with the network-shared vehicle system consisting of a battery charge station, vehicle station, and cloud network adaptation providing vehicle follow-up and tracking.

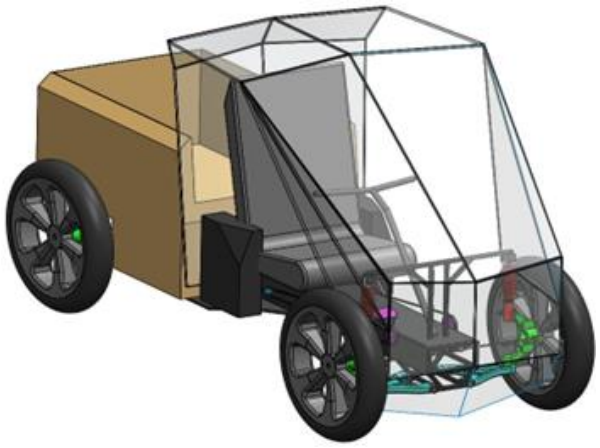

Figure 1. Pedal Assisted Cargo E-Quadricycle

In literature studies, electric vehicles are investigated based on specific powertrain system modeling details. Qin et al. [1] studied wheel motor modeling to improve driving comfort. They modeled 'Dynamic vibration absorbing structure (DVAS)' to provide more efficient vibration reduction. Abu Bakar et al. [2] investigated an active suspension system to evaluate the vehicle's ride and handling performance. They focused on evaluating two different weight distribution models 60:40 for normal vehicles and 40:60 for electric vehicle conversion. Jiang et al. [3] investigated solving unbalanced electromagnetic force in hub motors resulting in the deterioration of the dynamic performance of the electric vehicle. Therefore, the semi-active new model and Kalman filter are designed to provide the required state variables for the controller. Then, the proposed control algorithm is simulated to test random road excitations. Martinez and Tavernini [4] studied the proposal of friction brake torque estimation to simplify torque blending, and improve energy recovery and driving safety. In their model, the estimation is performed using the extended version of the Kalman Filter. Velmurugan et al. [5] used a GA (genetic algorithm) to estimate the vibration values and compared these values to experimental test data for further analysis of driving comfort related to the health risks in a suspended cabin tractor semi-trailer.

The popular preference is using electro-mobility vehicles under sheared autonomous usage. For this reason, deep learning tools and optimization algorithms are seriously performed to obtain the most optimized system under various traffic conditions [6]. Janiaud et al. [7] studied the electric powertrain simulation developed under Matlab-Simulink, intending to optimize performances and powertrain efficiency. The modeled system is used to choose battery technology and dimensions according to criteria and driving cycles. Hu et al. [8] investigated and studied the BMS control and energy consumption review based on the road-slope conditions including up-hill and down-hill conditions. Eckert et al. [9] studied different EV drivelines based on the different configurations. They used GA (Genetic Algorithm) to perform electric engine vs. reduction (transmission) gear ratio optimization.

In this study, the used suspension system is divided into two different systems. Macpherson suspension system type is designed for the front suspension system as independent, and the Wishbone independent suspension system is accepted for the rear section of the vehicle (Fig. 2). The reasons for selecting independent suspension systems consist of vehicle weight and different kinds of road profiles in the possible driving regions. In the study the mechanical inputs for both suspension system types are considered as same, therefore the stiffness and damping properties are represented as the same for each unique suspension system side of the wheel.

The dependent suspension systems for these vehicles have disadvantages in terms of vehicle comfort and NVH (noise, vibration, and harshness) phenomenon. Also, the independent suspension systems provide more strength and a consistent chain or pulley system which enables driver-dependent pedal force control.

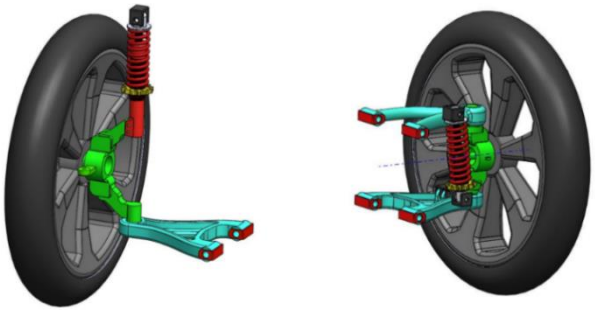

a) Macpherson - Front b) Wishbone - Back

Figure 2. Suspension System Used in the Design

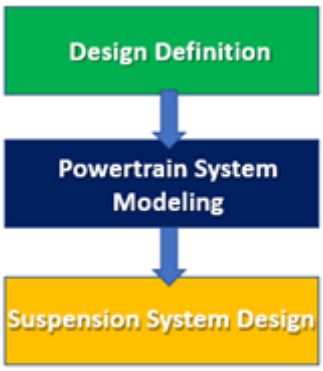

Figure 3. The methodology followed in the Study

Figure 3 illustrates the methodology followed during the study. The system is first designed with geometrical and constructive boundary conditions. As the next step, the powertrain system model is designed with considering electric motor excitation and pedal-assisted system details. This modeling method ensures a robust and endured system that enables to start of the vehicle in severe hill-start conditions. As the next step the suspension system design is performed and the system outputs are obtained by considering vehicle stability and dynamical operation limits. Pedal-assisted EMM vehicles (Pedelecs) have been rarely investigated in the scientific literature, also pedal-assisted E-Quadricycle system design is not deeply investigated considering specific designs such as pedal-assisted cargo E-Quadricycles. This study presents the specific design development that is produced for widely used markets such as consumer goods transportation etc. Because the passive suspension system is handled, the energy consumption effect of the suspension system is ignored during this study. The road condition is also accepted as mild severity corresponds to mostly low road incline and mild rolling resistance coefficient.

2. System Model Introduction

In this section, the system modeling is performed by considering geometrical boundaries. Table 1 indicates the model input data used in the design. The vehicle weight is 260 kg in total including additional weights and driver weight. The motor used in the design has a 250 W continuous power rate, the maximum power takes 940 W max during hill start conditions.

Table 1. Modeling data for physical model

Definition	Description
Nominal Voltage (V)	48
Max. Voltage (V)	52
Nominal Current (I)	14
Max. Allowed Current (I)	21
Battery Capacity (Wh) Cut-Off Voltage (V)	672 35
Driver Weight (kg)	80
Vehicle Weight (kg) Additional Weight (kg)	100 80
Maximum Weight (kg)	260
Tire Diameter (m)	0.50
Motor Nominal Power (W)	250
Motor Max. Power (W)	940
Max. Wheel Torque (Nm)	150
Nominal Voltage (V)	48
Max. Voltage (V)	52

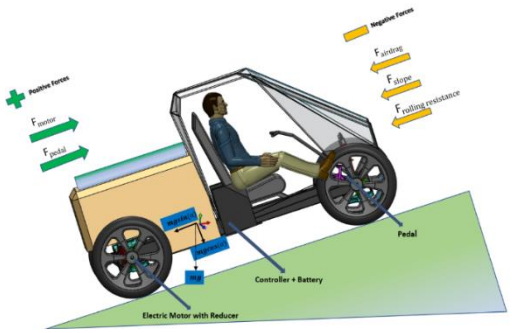

Figure 4. Effected Force for Hill Start

Figure 4 shows the hill start condition for the pedal-assisted E-Quadricycle vehicle having additional pedal force. Equation 1 explains the net force generated mainly by the electric motor and pedal force and sourced from Newtonian Mechanics. The force diagram on the related image is shown from the CoG (Center of Gravity), normal force, and slope forces. In this study the simulation is

performed at one second to simulate hill-start condition, therefore $F_{Airdrag}$ and F_{Slope} negative forces are not taken into account.

$$M\frac{dv}{dt} = +F_{Motor} + F_{Pedal} - F_{Airdrag} - F_{rolling\ resistance} \quad (1)$$

Pedal force is the source for additive excitation, and the ratio between the Crankset and Casette is important for straight, slope, hill, traffic jam, daily driving etc. conditions in bike use. Equation 2 and Equation 3 show the formula for how the pedal torque and force are created in the designed system. F_{Pedal} indicates the force provided when the driver pushes the driving pedal during rotational movement. As can be seen in the model, the Pedal force can be obtained maximum at Position B due to the moment effect (Figure 5). T_{Pedal} is the obtained torque, which is transmitted to the cassette gear set according to the gear ratio between the crankset and cassette. Figure 5 also explains the logic of additional force provided by the pedal, and also shows the pedal location of the modeled real E-Bike model including the PAS (Pedal Assist System) magnetic set-up.

$$T_{Motor\ (Nm)} = F_{Motor}\ r_{Tire} \quad (2)$$

$$T_{Pedal} = F_{Driver(Fy)} L_{Perpendicular\ Distance} \quad (3)$$

$F_{\mathbf{Airdrag}}$, $F_{\mathbf{Slope}}$, and $F_{\mathbf{Rolling\ Resistance}}$ are the negative forces operated against excitation forces. $F_{\mathbf{Airdrag}}$ can be defined as indicated in Equation 4. $P_{\mathbf{Air}}$ represents the air density of the environment where a bicycle is used. A is the projected area encounter to driving direction. $C_{\mathbf{D}}$ is the Air drag coefficient that depends on the transport configuration. Air drag force is also proportional to the square of the transport speed (v).

$$F_{Airdrag} = \frac{1}{2} P_{Air}\, A\, C_D\, v^2 \quad (4)$$

$F_{\mathbf{Slope}}$ is the negative force caused by the parallel force gradian of the total weights (driver and e-bike) multiplied by gravitational acceleration (g). $F_{\mathbf{Rolling\ Resistance}}$ also represents the slowing effects of the rubber tire. To calculate this factor perpendicular force is taken into account with the Rolling resistance coefficient ($C_{\mathbf{rr}}$) of the related road profile. Rolling resistance factor has a big importance and direct effect on energy consumption especially on asphalt, sandy, and gravel road types. Because of this reason, the energy consumption modeling based on the road profiles consists of a high level of criticality **[10]** Equations 5 and Equation 6 explain the detailed formula of these factors.

$$F_{Slope} = MgSin(\propto) \quad (5)$$

$$F_{Rolling\ Resistance} = MgCos\ (\propto) C_{rr} \quad (6)$$

In case the obtained net force is divided into total weight, acceleration is obtained (Eq. 7). If the obtained $\alpha_{\text{ vehicle}}$ value is subjected to integral operations, the velocity can be found as m/sn, km/h, and tire RPM versions.

$$\boldsymbol{F} = M_{\text{vehicle}}\, \alpha_{\text{ vehicle}} \quad (7)$$

Figure 6 indicates the one-dimensional modeling considering the hill-start condition. In this model, the battery power is converted to electric motor output torque according to RPM–Motor Efficiency Curve (2). The motor efficiency and obtained battery power multiplication have resulted in mechanical output torque. Figure 7 shows the modeling of Equation 1, which includes positive and negative forces. Figure 6 is part of Figure 7 by providing electric motor mechanical output torque. In this model, the electric motor torque generation and pedal force create the main positive torque values. According to the modeled Pedal Assisted Cargo E-Quadricycle, the designed system can be initiated till the 9° hill incline level without any pedal force support. In this model, tire radius (indicated in Table 1) is important in defining the magnitude of the generated force (Eq. 1).

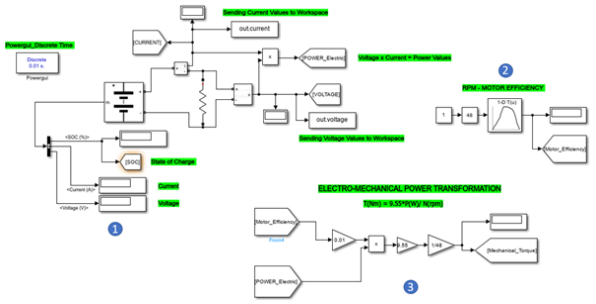

Figure 6. One-Dimensional Modeling for the Powertrain System

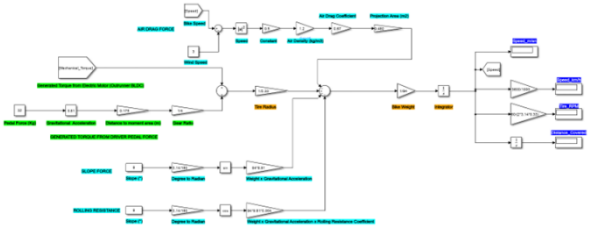

Figure 7. Mechanical Output Model of the System (Modeling of Eq. 1)

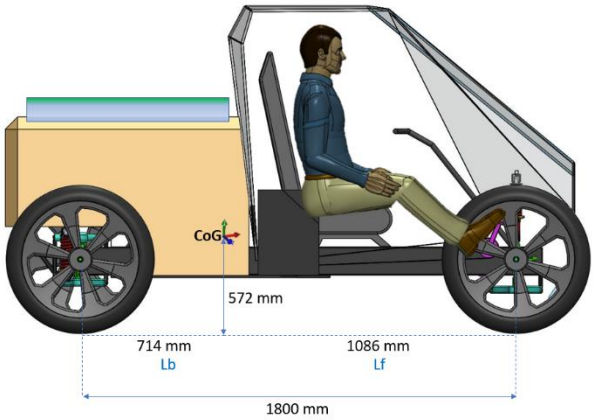

Figure 8. Geometrical data input for the suspension system

Figure 8 shows the CoG-dependent front and back axle distances designed in the model. The center of the vehicle mass is located closer to the rear axle due to more weight placed on the rear side such as the electric motor, additional weight, reducer, etc.

3. System Modeling

In this section, the suspension system specialized for Cargo E-Quadricycle (four-wheeler Cargo E-Bike) is modeled for the expected driving profile, and a mathematical basis is mentioned for the specified design.

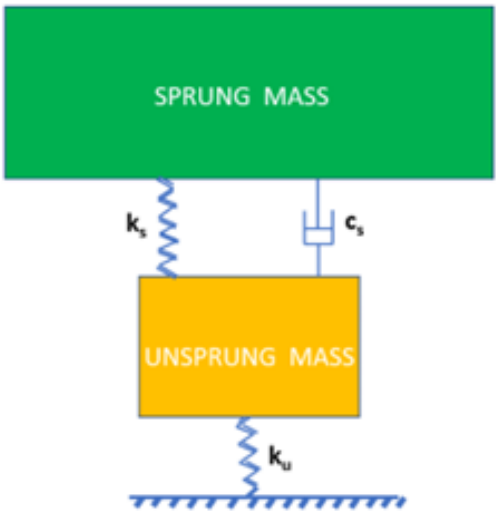

Figure 9. Quarter Vehicle based suspension system – Sprung vs. Unsprung Mass

Figure 9 shows the suspension base vehicle parts of the system. Sprung mass corresponds to the car body supported by the suspension system, conversely Unsprung mass explains the mass of the system parts which are not supported by damping and stiffness elements of the suspension system. Figure 10 shows the classification of damping types widely faced in system modeling of the industry. By selecting the damping types, NVH (Noise, Vibration, Harshness) should be also considered for the design. In Cargo E-Bike products especially Vibration and Harshness would be the key points to be in detail modeling.

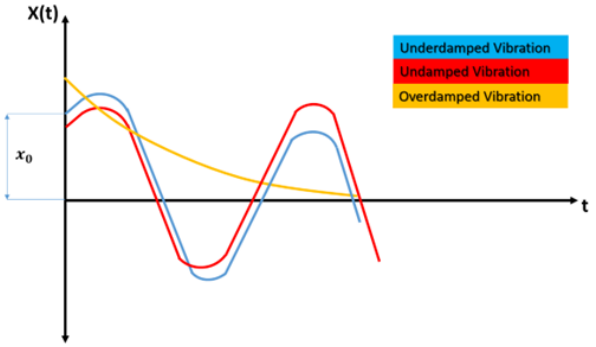

Figure 10. Damping types classifications

The design of the suspension system is considered as Underdamped as already expected damping characteristics of the other types of vehicles. The increase in natural frequency (F_N) increases acceleration transmissibility to the sprung mass and reduces ride comfort. Conversely, low natural frequency increases the static deflection of suspension springs and requires large suspension space due to soft springs. Thus, a value of natural frequency F_N = 1 to 1.5 Hz is used for passenger cars for better ride performance, and F_N = 2 to 2.5 Hz is used for performance cars on which ride is sacrificed for better handling **[11]**. To calculate feeling stiffness from the road to the total vehicle body, the Ride stiffness phenomenon (K_{rr}) is considered (Eq. 8). K_s ($\frac{N}{m}$) and K_u ($\frac{N}{m}$) correspond to Sprung Mass stiffness and Unsprung Mass stiffness as serially connected springs. To obtain the natural frequency (Eq. 9) near 1 (one) Hz and catch the geometrical limits the single suspension stiffness is selected as 2000 N/m providing 8000 N/m equal stiffness considering front and rear wheels, also the damping coefficient is selected as single 300 N.s/m with 1200 N.s/m equal damping value considering front and rear wheels. The equal wheel stiffness is selected 75000 N/m by considering 20” wheel size.

$$K_{rr} = \frac{K_s K_u}{K_s + K_u} \quad (8)$$

$$f_N = \frac{1}{2\pi}\sqrt{\frac{K_{rr}}{m}} \quad (9)$$

$$\zeta = \frac{C}{C_C} \quad (10)$$

$$\zeta = \frac{C}{2\sqrt{km}} \quad (11)$$

The design of the suspension system is requested as underdamped to provide riding and transportation comfort. Thus, to have underdamped damping characteristic, ζ should be provided as $\zeta = \frac{C}{C_C} < 1$ (Eq. 10). Based on the selected suspension parameters Table 2 is given. In the equal vehicle model, the equal damping ratio is found 0.41 showing underdamped behavior. The suspension natural frequency is found as 0.84 which is targeted to catch passenger car suspension frequency (1 Hz – 1.5 Hz) comfort instead of sport racing cars (2 Hz – 2.5 Hz).

Table 2. Suspension Parameters vs. System Properties

Definition	Description
Damping (N.s/m) – each suspension, C	300
Stiffness (N/m) – each suspension, K	2000
Equal Damping (N.s/m), C_E	1200
Equal Sprung Stiffness (N/m), K_S	8000
Equal Critical Damping, C_C ($2\sqrt{km}$)	2884
Equal Damping Ratio, ζ	0.41
Tire Stiffness (N/m), K_U	75000
f_{rr} (including Ks wheel stiffness), Hz	0.84

During dynamic conditions, the suspension response force is calculated via Equation 12. In this equation x, K, C and v represent in order; Contact Depth (m), Spring Stiffness $(\frac{N}{m})$, Damping Coefficient $(N.\frac{s}{m})$, and Compression Speed (m/sn).

$$F_{suspension} = x\,K + C\,v \quad (12)$$

Figure 11 shows the random driving faced with curbs in specific obstacle dimensions. In the chart, the Quarter vehicle mass, modeled with hysteresis and stiffness factors, is performed to different heights of curbs. Equations 13, 14, and 15 explain the way of reaching suspension pressing distance and velocity.

Figure 12 explains the suspension system model of the vehicle. F_{motor} and F_{pedal} represent the positive propulsive Forces, which affect rotating the vehicle counterclockwise in I_{yy} coordinate (pitch effect on counterclockwise direction), whereas F_{break} results in rotating in the clockwise direction, namely pitch effect on clockwise.

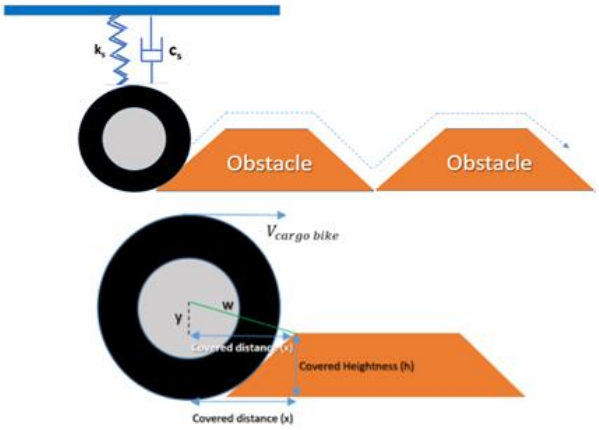

Figure 11. Cargo E-Bike Suspension System Operation

$$w^2 = x^2 + y^2 \quad (13)$$

$$\Delta t = \frac{x}{V_{cargo\ bike}} \quad (14)$$

$$V_{spring\ compression} = \frac{h}{\Delta t} \quad (15)$$

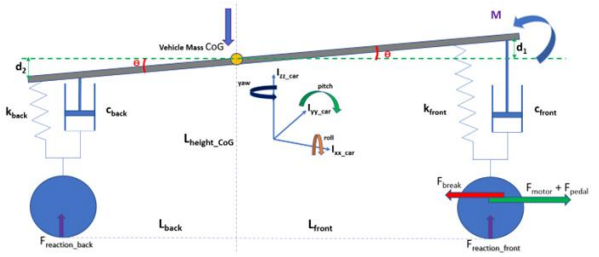

Figure 12. Suspension System Modelling Considering Inertial Forces

Table 3. Modeling Inputs for Suspension Design

Definition	Description
I_{car}	74.6 kg.m^2
L_{back}	0.714 m
L_{front}	1086 m
$L_{heightness}$	0.572 m
t < 5 second	600 N
t >= 5 & t <10	0 N
t>= 10 & t<15	-200 N

Table 3 shows the geometrical boundary conditions and performed excitation forces during the simulation. Positive force (600 N) represents the F_{motor} and F_{pedal} by considering the electric motor's maximum torque and additional pedal force proportional to the wheel tire. This force value is considered representative and the system is run to see the system's behavior. Negative force (-200 N) represents the brake force to see the system behavior in brake conditions. During these movements because of the small displacements d_1 and d_2 are considered as $Sin\theta \approx \theta$. Equation 16 shows the stability of the system centered on the Vehicle's Center of Gravity according to Newton 's 2nd law.

$F_{motor} + F_{pedal}) L_{height\_CoG} + (-L_{back}\ \boldsymbol{\theta}\ K_{back}) + L_{front}\ \boldsymbol{\theta}\ K_{front} + (-L_{back}\ \dot{\boldsymbol{\theta}}\ C_{back}) + L_{front}\ \dot{\boldsymbol{\theta}}\ C_{front} = I_{yy\_car}\ \ddot{\boldsymbol{\theta}}$ (16)

F_{motor} and F_{pedal} are named F_{total} during the next equations. To obtain the State-space model of the stability equation, the final stability equation is written based on the compression and extension angle θ in Equation 17.

$$\ddot{\theta} = F_{total}\frac{Lheight}{Iyy\_car} + \dot{\theta}\frac{C}{Iyy\_car} + \theta\frac{K}{Iyy\_car} \quad (17)$$

The state of the stability is defined as Θ angle, therefore State-space model of now defined $X_1 = \Theta$ and $X_2 = \dot{\theta}$. A matrix corresponds to the state definition, and the B matrix also defines input factor F_{total} which equals the sum of F_{motor} and F_{pedal}.

Equation 18 shows the State-space base format used in this study. A corresponds to the matrice of state definition, while B is the system input matrix which is indicated with u. In this State-space format, electric motor torque and pedal force are not considered separately, instead regardless of separate partially controlling and managing, the driving torque is considered in total.

$$\dot{x} = Ax + Bu$$

$$\begin{bmatrix}\dot{x_1}\\ \dot{x_2}\end{bmatrix} = \begin{bmatrix}0 & 1\\ \frac{K}{Iyy\_car} & \frac{C}{Iyy\_car}\end{bmatrix}\begin{bmatrix}x_1\\ x_2\end{bmatrix} + \begin{bmatrix}0\\ \frac{Lheight_{CoG}}{Iyy_{car}}\end{bmatrix}F_{total} \quad (18)$$

In steady state conditions, there is no positive or negative acceleration exists, the suspension system composed of spring and damper is just pressed due to vehicle mass. Equation 19 explains the static condition and the equality for the mass and suspension system reaction forces. In case there is no acceleration occurs resulting in zero force occurrence, there is no more press occurring on the spring.

$$\sum F_{net} = \text{Vehicle Mass} - (F_{reaction\_back} + F_{reaction\_front}) \quad (19)$$

In dynamic conditions, the suspension system prevents the vehicle from tilting and falling over movement. $F_{motor} + F_{pedal}$ creates the bending moment resulting in leaning the passenger back direction, whereas F_{break} force generates the bending moment resulting in leaning forward for the passengers (Fig.13).

In Figure 14, the system can be explained as d_1 and d_2, and F_{DB} and F_{DF}. Then, d_1 (front)and d_2 (back) explain the shift amount of the front suspension system proportional to $Sin\boldsymbol{\theta}$(Eq.20, and Eq. 21), so F_{DF} (front) and F_{DB} (back) indicate the total reaction force generated in the suspension system created due to spring stiffness and damper viscosity (Eq. 22, and Eq. 23).

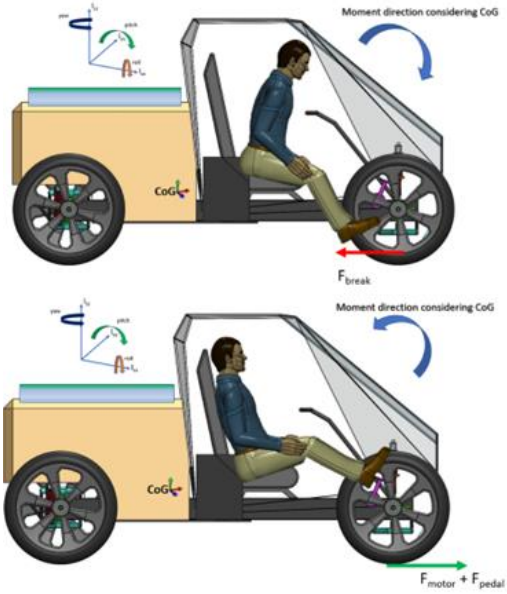

Figure 13. Comparison for moment direction considering CoG created by F_{break} and $F_{motor} + F_{pedal}$

$$d_1 = L_{front}\ Sin\boldsymbol{\theta} \quad (20)$$

$$d_2 = L_{back}\ Sin\boldsymbol{\theta} \quad (21)$$

$$F_{DF} = L_{front}\ Sin\boldsymbol{\theta}\ K_{front} + L_{front}\ Sin\dot{\boldsymbol{\theta}}\ C_{front} \quad (22)$$

$$F_{DB} = -(L_{back}\ Sin\boldsymbol{\theta}\ K_{back} + L_{back}\ Sin\dot{\boldsymbol{\theta}}\ C_{back}) \quad (23)$$

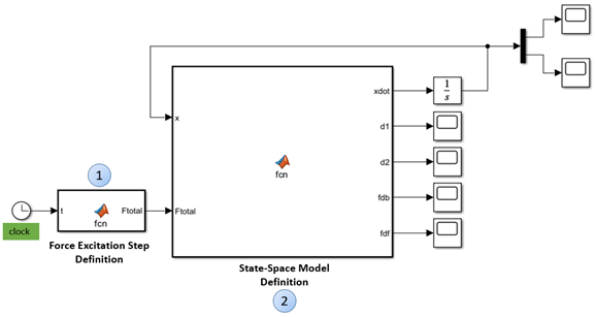

Figure 14. One-Dimensional Modeling for Suspension Design

Figure 14 explains the general chart of the Matlab Function model prepared in Simulink. The clock module provides the time range of the excitation steps. Force excitation step block (block 1) includes the positive and negative forces based on the time arranged by the Clock module. State-Space Model block (block 2) includes the parameters to solve the State-Space system identification method (see Eq.

18). Block 1 gives the F_{Total} force excited to drive the vehicle. As given in Table 3 the Cargo E-Bike is excited with 600 N positive force representing F_{motor} and F_{pedal} for 5 seconds, and driven for 5 seconds without additional force, then 5 seconds the brake force is applied as -200 N. Because the geometrical design is not symmetric (see Table 3), the system response for front and rear suspension is not expected as with the same outputs. Block 2 includes the State-Space form of Equation 16 into Equation 18. The system is written under the Matlab function in the Simulink module.

4. Results and Discussions

In this section, the analysis results are investigated and discussed. Figure 15 shows the angular displacement and angular velocity behavior of the suspension angle Θ (see Eq. 18) during the 20-second run. The angular definitions are indicated in the Radian unit as $\text{Sin}(\Theta) \approx \Theta$ in relatively small angles.

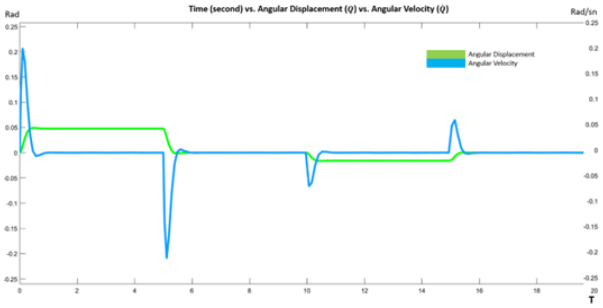

Figure 15. System State behavior – Angular Displacement Θ vs. Angular Velocity $\dot{\theta}$

As seen in the graph, the angular displacement reached the maximum of 0.047 radians in positive excitation provided by F_{motor} and F_{pedal} (in total 600 N) creating a bending moment in counter clock-wise, in parallel the maximum angular velocity is seen as 0.21 Rad/sn during first excitation. The start-up condition creates a bending moment in counter clock-wise (see Fig. 13). Thus, during the first 5 seconds the front suspension system (D_1) behaviors in extension to the positive direction (up), while the rear suspension system (D_2) is pressed into the negative direction (down). The displacement of the springs is pressed just belongs to vehicle system behavior without considering vehicle mass (Eq. 19) because the vehicle mass is compensated in static condition.

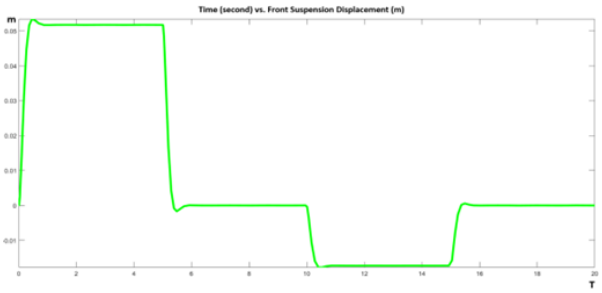

Figure 16. Front suspension system displacement (m) vs. time (t) – d1

Figure 16 shows the front suspension system behavior subjected to positive and negative force excitations. At the first initial condition, the front suspension system is seen with 0.056 m extension, while in Figure 17 it can be seen that the rear suspension system is pressed with 0.035 m in the negative direction. Between 5 seconds to 10 seconds, the front and rear suspension systems appear to come balanced position without any extension and pressing. Between 10 seconds to 15 seconds, the vehicle is subjected to a brake force of -200 N. This motion creates a bending moment in a clockwise direction (see Fig. 13). D_1 (front suspension – Fig. 16) is squeezed up to -0.02 m (negative direction) while the rear suspension (Fig. 17) is extended to 0.01 m in a positive direction.

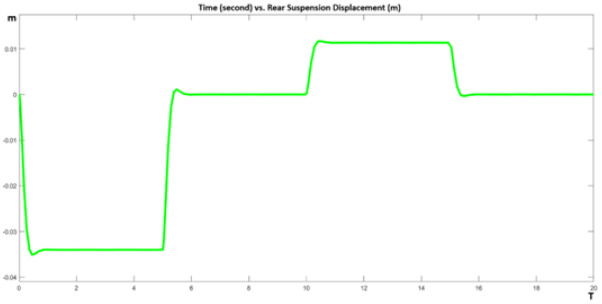

Figure 17. Rear suspension system displacement (m) vs. time (t) – d2

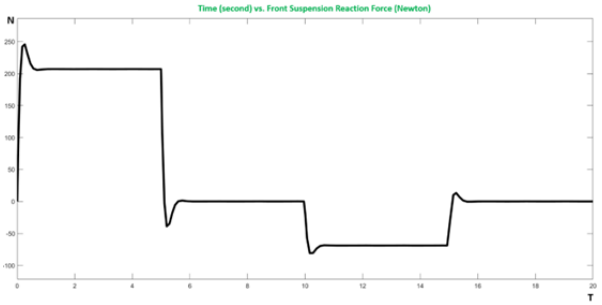

Figure 18. Front suspension reaction force (N) vs. time (t) – fdf

The reaction force of the suspension is explained in Equation 12. As indicated in this equation, the reaction force is proportional to

suspension squeezing time multiplication by damping coefficient that means in high longitudinal velocities the suspension reaction force attempts to increase. Figure 18 and Figure 19 show the reaction forces belonging to the front and rear suspension respectively.

As seen in Figure 18, the front suspension creates a maximum 245 N reaction force in the first 5 seconds dependent on 600 N positive force occurring by motor and pedal forces. Between 5 seconds to 10 seconds, the suspension dynamic reactions belong to motion-based reaches balanced condition. Rear suspension (Figure 19) is subjected to 162 N reaction force in a negative direction during the first 5 seconds, then stabilized its condition between 5 to 10 seconds.

Due to the bending moment effect clockwise between 10 seconds to 15 seconds, the front suspension is pressed into a negative direction. In this condition, the front suspension creates a 78 N maximum force, while the rear suspension results in a 49 N maximum dynamical force in the upward direction. The system data is summarized in Table 4, considering peak obtained values.

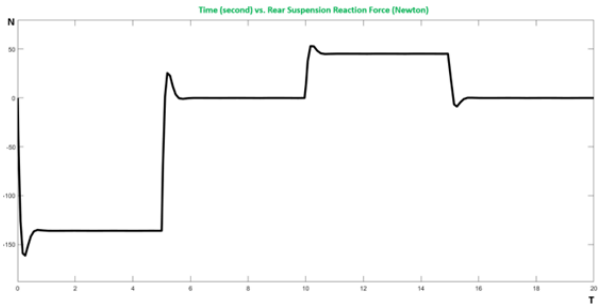

Figure 19. Rear suspension reaction force (N) vs. time (t) – fdb

Table 4. System Response Values Considering Motion Direction

	0-5 sec	5-10 sec	10-15 sec
Front suspension system displacement D_1 (m)	0.056	0	-0.02
Front suspension system displacement D_2 (m)	-0.035	0	0.01
Front suspension system total reaction force (N)	245	0	-78
Rear suspension system total reaction force (N)	-162	0	49

5. Conclusions

In this study, the pedal-assisted Cargo E-Quadricycle (Pedelec EMM) is modeled, and the passive suspension system is designed by considering vehicle properties. The suspension dynamic responses are simulated by considering the flat road and hill-start conditions without jumping over bumper and curb. At the design phase, the quarter vehicle model parameters are defined as sprung and unsprung mass considering natural frequency to provide driving comfort. As the next step, based on the boundary conditions the suspension system design is modeled considering vehicle stability in pitch movement (I_{yy}). Then, the State-Space model is created based on the dynamic motion equation. The obtained model results verified the used spring and damper system characteristics accuracy. The methodology presented in this study provides an innovative approach for Pedal-Assisted system modeling for EMM vehicles.

Acknowledgment

This study is supported by TUBITAK under grant number 2220390 entitled “Mobile networked ergonomic modular high-torque urban electric transport vehicle” project.

6. References

1. Qin, Y., He, C., Ding, P., Dong, M., Huang, Y., “Suspension Hybrid Control for In-Wheel Motor Driven Electric Vehicle with Dynamic Vibration Absorbing Structures”, IFAC PapersOnLine, Vol. 51, Issue.31, pp. 973–978, 2018.

2. Abu Bakar, S. A., Masuda, R., Hashimoto, H., Inaba, T., Jamaluddin, H., Rahman, R. A., “Active Suspension System in Improving Ride and Handling Performance of Electric Vehicle Conversion”, International Journal of Electric and Hybrid Vehicles, Vol. 4, Issue. 1, https://doi.org/10.1504/IJEHV.2012.047877, pp. 24-53, 2012.

3. Jiang, H., Wang, C., Li, Z., Liu, C., “Hybrid Model Predictive Control of Semiactive Suspension in Electric Vehicle with Hub-Motor”, Applied Sciences, Vol. 11(1), Issue. 382, https://doi.org/10.3390/app11010382, 2021.

4. Martinez, C. M., Tavernini, D., “Modelling and Estimation of Friction Brake Torque for a Brake by Wire System”, IEEE Conferences, 10.1109/IEVC.2014.7056105,

2014.
5. Velmurugan, P., Kumaraswamidhas, L., Sankaranarayanasamy, K., “Optimization of suspension parameters based on simulation of ride comfort in vehicle development”, International Journal of Vehicle Noise and Vibration, Vol. 8, Issue. 2, pp. 152–165, 2012.
6. Kim, S., Lee, U., Lee, I., Kang, N., “Idle vehicle relocation strategy through deep learning for shared autonomous electric vehicle system optimization”, Journal of Cleaner Production, Vol. 333, Issue.130055, 2022.
7. Janiaud, N., Vallet, F., Petit, M., Sandou, G., “Electric Vehicle Powertrain Simulation to Optimize Battery and Vehicle Performances”, IEEE Conference on Vehicle Power and Propulsion (VPPC)-IEEE Online Journal, 978-1-4244-8218-4, 2011.
8. Hu, T., Li, Y., Zhang, Z., Zhao, Y., Liu, D., “Energy Management Strategy of Hybrid Energy Storage System Based on Road Slope Information”, Energies, Vol. 14, doi:10.3390/en14092358, 2021.
9. Eckert, J., Silva, L., Costa, E., Santiciolli, F., Dedini, F., Correa, F., “Electric vehicle drivetrain optimization”, IET Electrical Systems in Transportation, Vol. 7, Issue: 1, pp. 32-40, 2017.
10. Meyer, D., Kloss, G., Senner, V., “What is slowing me down? Estimation of rolling resistances during cycling”, Procedia Engineering, Vol. 147, pp. 526-531, 2016.
11. Dharankar, C., Hada, M. K., Chandel, S., “Performance improvement of passive suspension of vehicles using position dependent damping”, International Journal of Vehicle Performance, Vol. 4, No: 1, https://doi.org/10.1504/IJVP.2018.088802, 2018.
12. Genc, M. O., Kaya, N., “Design and verification of elastomer spring damping system for automobile powertrain systems”, Journal of the Faculty of Engineering and Architecture of Gazi University, Vol.35, Issue. 4, pp. 1957-1971, 2020.
13. Hwang, S. J., Chen, J. S., Liu, L., Ling, C. C., “Modelling and Simulation of a powertrain system with automatic transmission”, International Journal of Automobile Design, Vol. 23, Issue. 1, DOI:10.1504/ IJVD.2000.001888, 2000.
14. Miyasato, H., Siminatto, G., Junior, M., “Linear Powertrain Models for NVH Phenomena Evaluation”, International Symposium on Dynamic Problems of Mechanics, pp. 143-152, Buzios-Brazil, 2013.
15. Dharankar, C., Chandel, S., “Performance improvement of passive suspension of vehicles using position dependent damping”, International Journal of Vehicle Performance. Vol. 4, Issue. 1, DOI: 10.1504/IJVP.2018.088802, 2018.